International Journal of Microwave and Wireless Technologies

cambridge.org/mrf

A Ka-band slant-polarized two-dimensional phased array

Ganlin Feng, Junfeng Shi, Yifei Mu, Huan Yang, Xingfan Wu and Jiawei Xu

Department of Microwave Engineering, Xi'an Electronic Engineering Research Institute, Xi'an, China

Research Paper

Cite this article: Feng G, Shi J, Mu Y, Yang H, Wu X, Xu J (2026) A Ka-band slant-polarized two-dimensional phased array. *International Journal of Microwave and Wireless Technologies* **18**(2), 273–282. https://doi.org/10.1017/S1759078726103092

Received: 24 October 2025
Revised: 7 March 2026
Accepted: 13 March 2026

Keywords:
two-dimensional phased array; slant polarization; polarizer

Corresponding author: Ganlin Feng;
Email: ganlinfeng09@126.com

Abstract

Based on practical requirements, this paper presents the design, fabrication, and experimental validation of a Ka-band wideband two-dimensional (2D) phased array antenna with 45° slant polarization. The array integrates a polarizer with 28 six-element metallic Vivaldi linear subarrays. To the best of the authors' knowledge, no previous work has reported the engineering implementation of a polarizer-integrated 2D phased array at Ka-band, as existing studies are limited to single elements or one-dimensional arrays. Measured results show that the array achieves an active Voltage Standing Wave Ratio (VSWR) below 2.6 over 32–40 GHz, with a gain exceeding 25.5 dBi. It supports wide-angle scanning up to ±50° in the azimuth plane and ±30° in the elevation plane, with a scan loss not exceeding 3 dB across the entire scanning range. Furthermore, the amplitude difference between horizontal and vertical polarization components remains within 2.9 dB throughout the scanning range, confirming desirable slant polarization characteristics.

Introduction

Slant-polarized antennas, capable of radiating equal-power horizontal and vertical electromagnetic waves to form a 45° slant polarization, have found applications not only in military systems (e.g., ground-based communications and electronic countermeasures) but also in mobile communication base stations, where they provide more symmetrical propagation characteristics than purely vertically or horizontally polarized antennas [1].

The simplest way to achieve slant polarization is to place the linearly polarized element at an angle of 45° [2–9]. Similarly, if two linearly polarized elements are placed at angles of 45° and 135°, respectively, dual slant-polarized characteristics can be realized [10–14]. Although this method is simple and easy to implement, the slant-polarized characteristics usually get worse when the array scans at large angles. Another method is to excite the horizontally polarized and vertically polarized elements with equal amplitude and phase to form slant 45° polarization [15], which requires a power divider network. In addition, the slant polarization can be obtained by loading a polarization converter which can convert the horizontally or vertically polarized electromagnetic waves to slant polarization [16–19]. This method can maintain good slant polarization purity when scanning at large angles, but it increases the height of the antenna. However, the antennas proposed in these papers are not two-dimensional (2D) phased arrays. Based on the literature reviewed by the authors to date, research and applications related to achieving slant polarization by loading polarizers have primarily focused on antenna elements or one-dimensional (1D) phased arrays. Studies and engineering implementations of slant-polarized 2D phased array antennas loaded with polarizers are rarely reported.

In this paper, a Ka-band slant-polarized, 2D phased array antenna loaded with a polarizer is designed and fabricated. The radiating element is an all-metal Vivaldi antenna, chosen for its high structural strength and modularity. A 45° slant polarizer is integrated above the antenna array to achieve the desired polarization. Compared to the conventional method of rotating elements to a 45° orientation [20], this approach effectively mitigates the increase in cross-polarization during diagonal-plane scanning, which is typical of Vivaldi antennas [21]. The proposed array adopts a triangular lattice, operates over a bandwidth of 32–40 GHz, and maintains an active VSWR below 2.6 across the scanning range. Measurements show that the array achieves scanning ranges of ±50° in the azimuth plane (AZ-plane), which corresponds to the H-plane, and ±30° in the elevation plane (EL-plane), which corresponds to the E-plane. Within the scanning range, the amplitude difference between the horizontal polarization (H-pol) component and the vertical polarization (V-pol) component remains within 2.9 dB, and the maximum scanning gain loss is 3 dB. These results demonstrate excellent wide-angle scanning performance, confirming the array's suitability for modern radar and electronic warfare systems.

Antenna design

The all-metal Vivaldi antenna is composed of a radiating part (the flare notch) and a feeding part, as illustrated in Fig. 1(a). Similar to the PCB-based Vivaldi antennas, the radiating part

© The Author(s), 2026. Published by Cambridge University Press in association with The European Microwave Association.

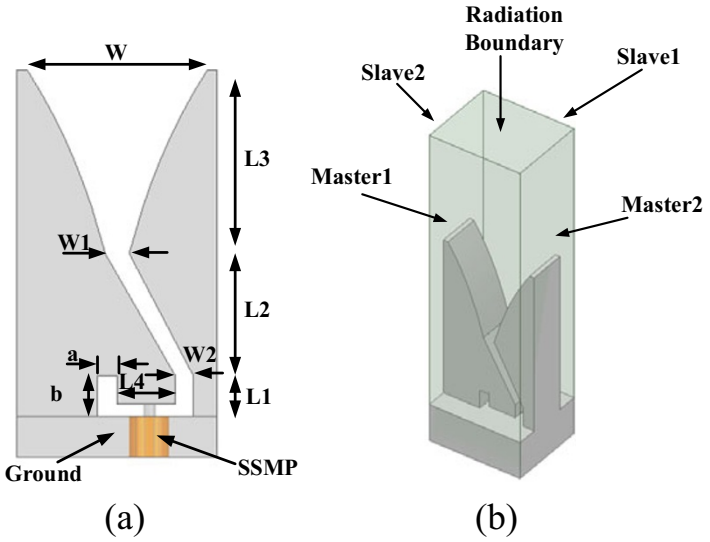


Figure 1. Metal Vivaldi element. (a) Side view of the element and (b) element simulation model.

Table 1. Model dimensions (mm)

W	*W*1	*W*2	*L*1	*L*2	*L*3	*L*4	*a*	*b*
4	1	0.6	1.5	2.5	3.5	2	1	1.5

employs an exponentially tapered aperture to achieve effective impedance matching. The feeding part is composed of a slot-line and a cavity, designed to achieve both impedance matching and energy transmission. Compared to microstrip-to-slot-line transition of traditional PCB-based designs [22] and the Marchand balun [23], the feeding part transfers energy directly from the coaxial connector into the slot-line. Furthermore, unlike previous element designs [21, 24–27], the proposed antenna removes the metal portion between the slot-line and the ground, integrating the feeding part with the ground. This integration thus liberates connector selection from the constraint of antenna thickness. The element is roughly $2/3\lambda$ in width, $1/3\lambda$ in thickness, and 1λ in height, where λ represents the wavelength at the high-frequency end of the band. The actual element lattice spacing is 4.2 mm × 5.0 mm, which is primarily determined by the requirement to suppress grating lobes within the operational scanning range.

The element was simulated and optimized with ANSYS using periodic boundaries, as shown in Fig. 1(b). Its optimized dimensions are summarized in Table 1. As shown in Fig. 2, the simulated VSWR remains below 2 across the entire band at broadside. Under scanning conditions, the VSWR is below 1.6 at +50° in the AZ-plane and below 2 at +30° in the EL-plane. These results confirm the element's good impedance matching across the operational bandwidth and within the specified scan range.

Array simulation

The array comprises 28 linear sub-arrays, each containing 6 elements. These sub-arrays were monolithically fabricated from aluminum using high-precision wire electrical discharge machining, achieving a dimensional tolerance of ±0.02 mm (Fig. 3).

Following the initial element design via unit-cell simulation under periodic boundary conditions, a full 28 × 6 array model

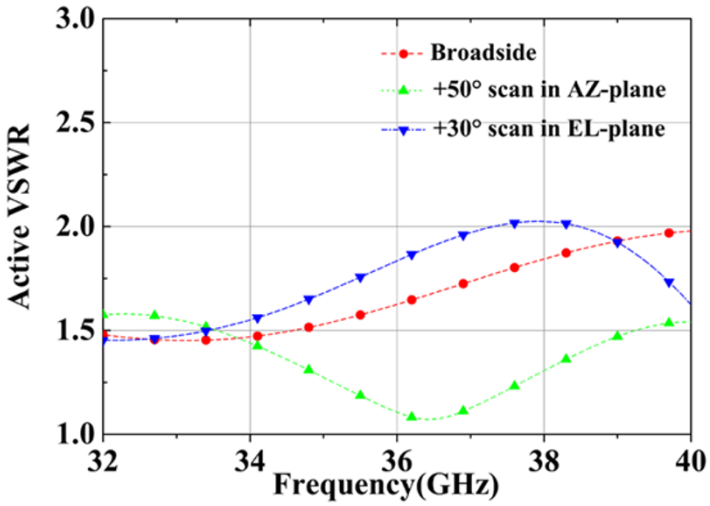


Figure 2. Simulated VSWR of element.

https://doi.org/10.1017/S1759078726103092 Published online by Cambridge University Press

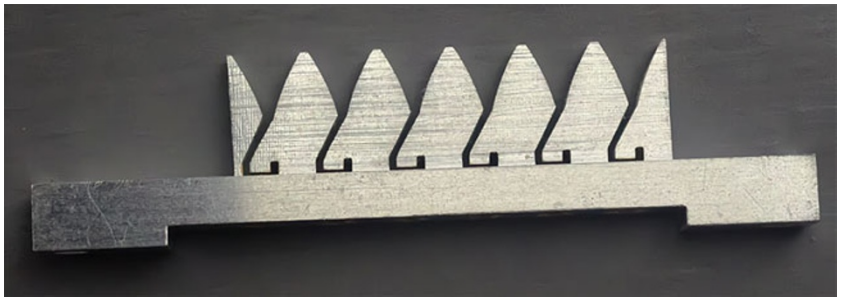


Figure 3. Six-element linear sub-array.

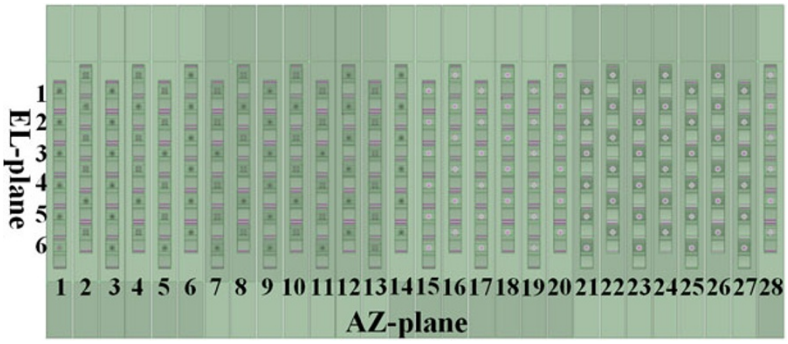


Figure 4. Top view of array simulation model.

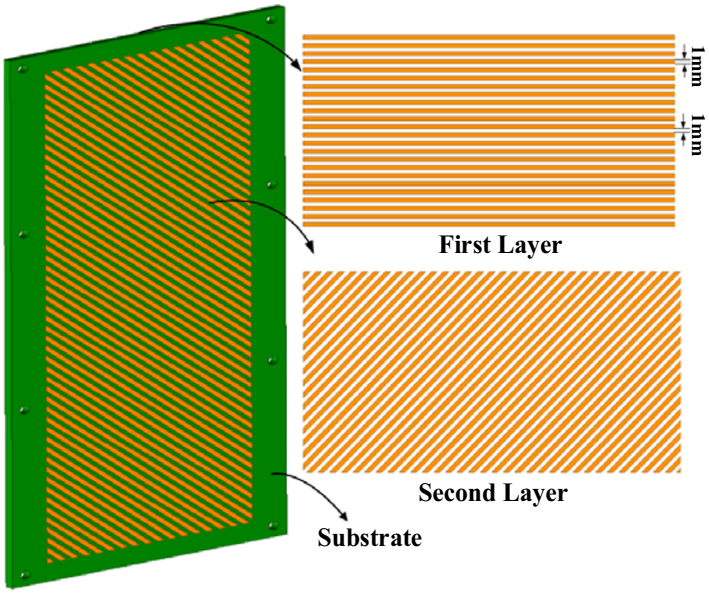


Figure 5. Geometry of the polarizer.

was constructed for more accurate full-wave analysis. The array is configured with 28 elements in the AZ-plane and 6 elements in the EL-plane. To accurately model the physical assembly, a 0.2 mm gap was introduced between adjacent linear sub-arrays in the simulation. The complete model is shown in Fig. 4.

The polarizer comprises two layers of metallic strips, as illustrated in Fig. 5. The strips in the first layer are perpendicular to the incident electric field, while those in the second layer are oriented at a 45° angle. Both layers have identical strip widths and inter-strip gaps of 1 mm. The dielectric between them is a Rogers 5880 substrate with a thickness of 1.5 mm.

The combined array and polarizer model is shown in Fig. 6. To accommodate the beam scanning range and the required placement height of the polarizer, the polarizer's aperture was enlarged relative to the array aperture.

The active VSWR of the six elements in the 14th azimuth column across the scanning range is shown in Fig. 7. The simulated values remain below 2.8 within the band, confirming acceptable impedance matching. Moreover, their variation trend agrees well with the unit-cell simulation results obtained under periodic boundary conditions (Fig. 2).

Figure 8 shows the simulated, normalized H- and V-pol radiation patterns versus scan angle. Across the entire band and scan range, the amplitude difference between the two components remains below 2.6 dB, demonstrating excellent purity of the 45° slant polarization.

https://doi.org/10.1017/S1759078726103092 Published online by Cambridge University Press

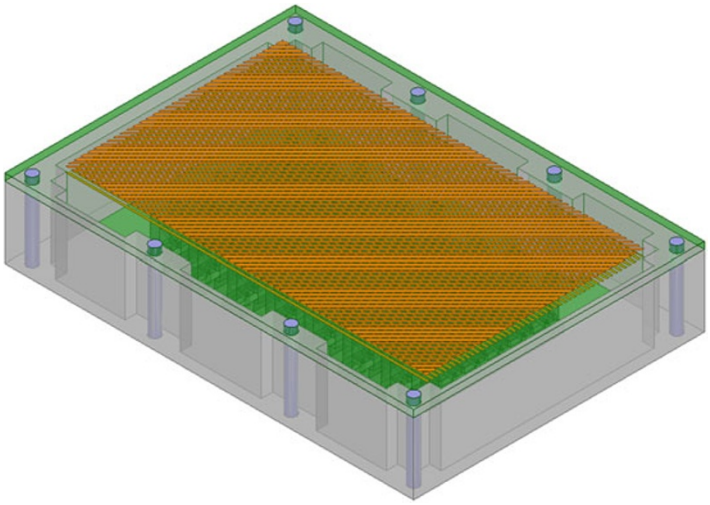


Figure 6. Simulation array model with polarization converter.

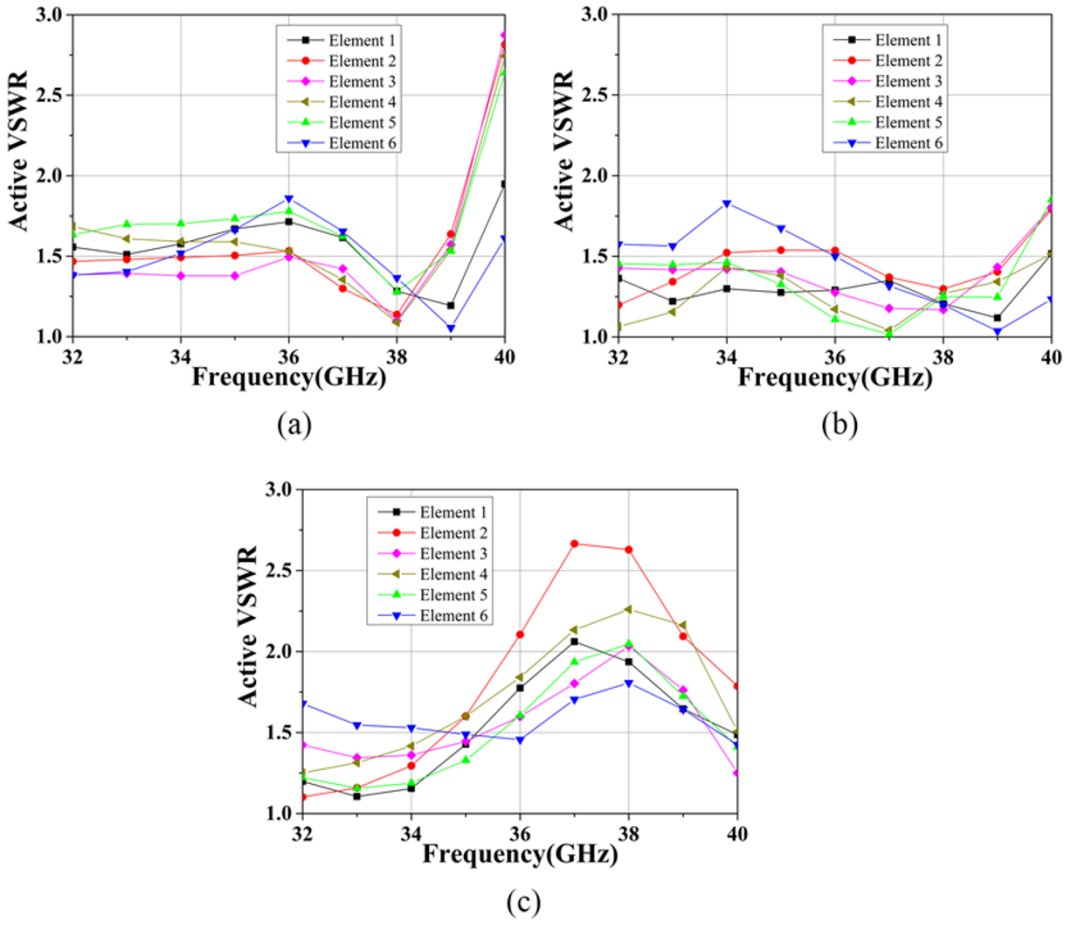


Figure 7. Simulated active VSWR of center six-element sub-array for (a) broadside radiation, (b) +30° scan in EL-plane, and (c) +50° scan in AZ-plane.

Results and discussion

A 28 × 6 array prototype, measuring 117.6 mm × 33 mm × 7.5 mm, was fabricated. Figure 9 shows photographs of the array; the polarizer is omitted to reveal the layout of the sub-arrays. The active VSWR was measured using an Agilent N5244A vector network analyzer, while the radiation patterns and gain were measured in a microwave anechoic chamber. For the pattern measurements, each linear sub-array was connected to a six-channel T/R module to enable independent control of the amplitude and phase of each element.

The active VSWR was measured for each element using an S-parameter synthesis procedure [23]. Results for three representative elements are presented in Fig. 10: edge element 1 (Row 1, Column 1), edge element 4 (Row 4, Column 1), and center element

https://doi.org/10.1017/S1759078726103092 Published online by Cambridge University Press

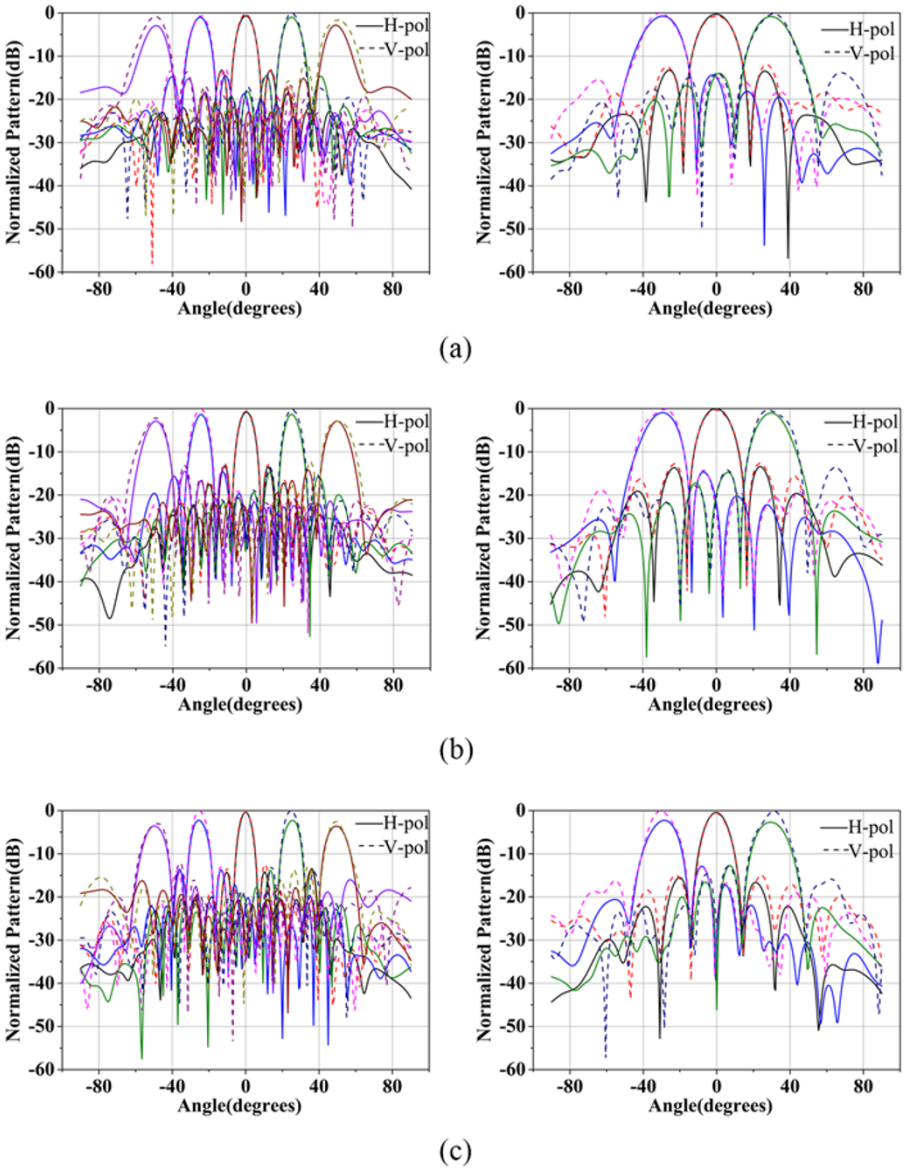


Figure 8. Simulated normalized patterns at broadside and scan angles of ±25° and ±50° in the AZ-plane and ±30° in the EL-plane. (a) 32 GHz in AZ-plane (left) and EL-plane (right), (b) 36 GHz in AZ-plane (left) and EL-plane (right), (c) 40 GHz in AZ-plane (left) and EL-plane (right).

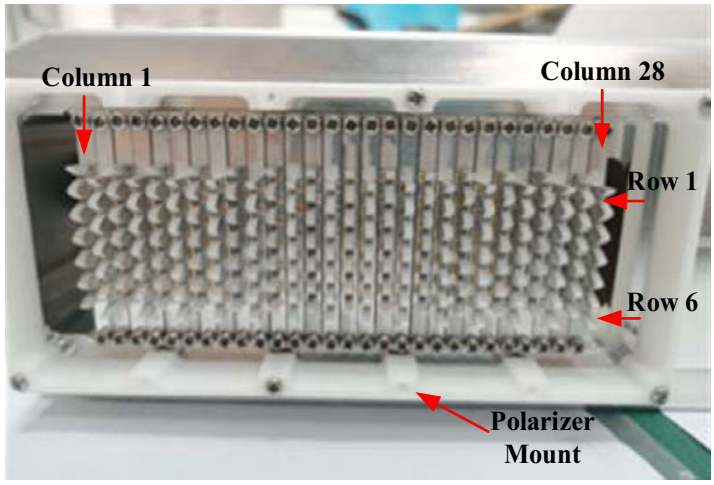


Figure 9. 28 × 6 element array constructed from modular sub-arrays.

https://doi.org/10.1017/S1759078726103092 Published online by Cambridge University Press

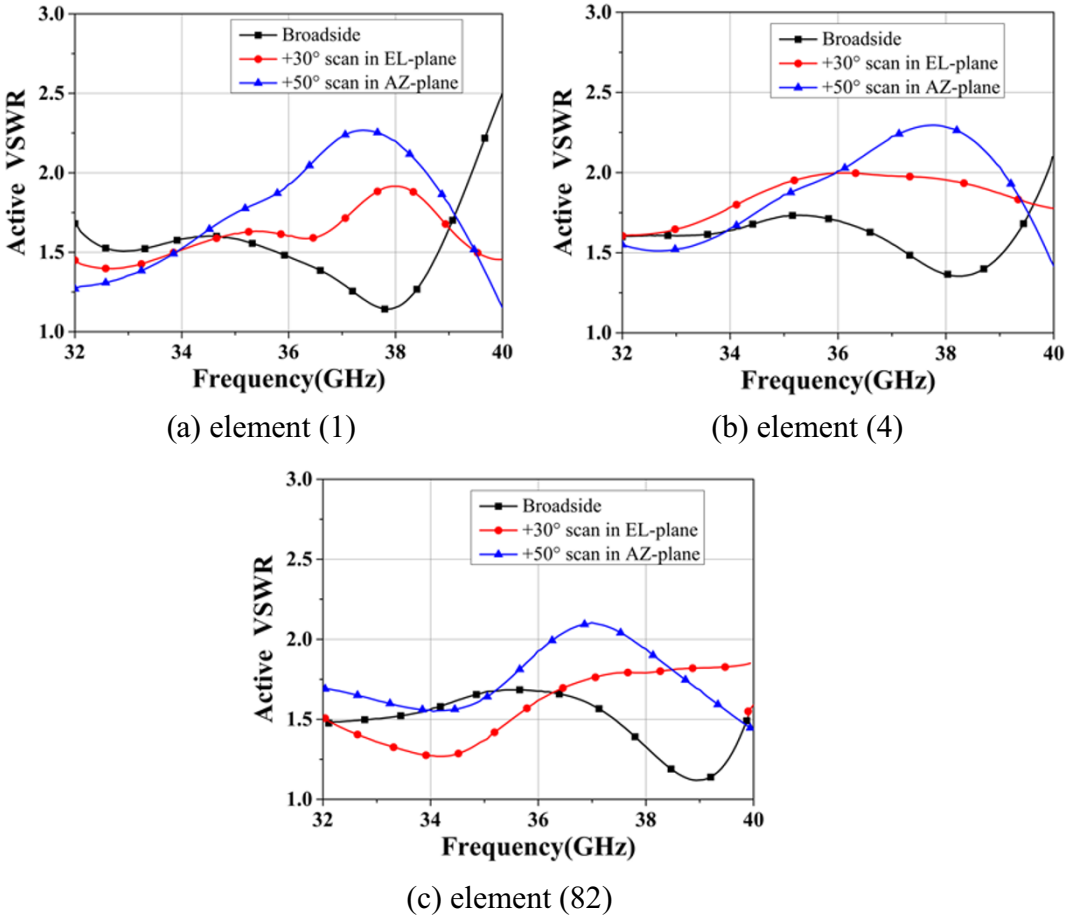


Figure 10. Measured active VSWR for elements (1), (4), and (82) in the 28 × 6 element array.

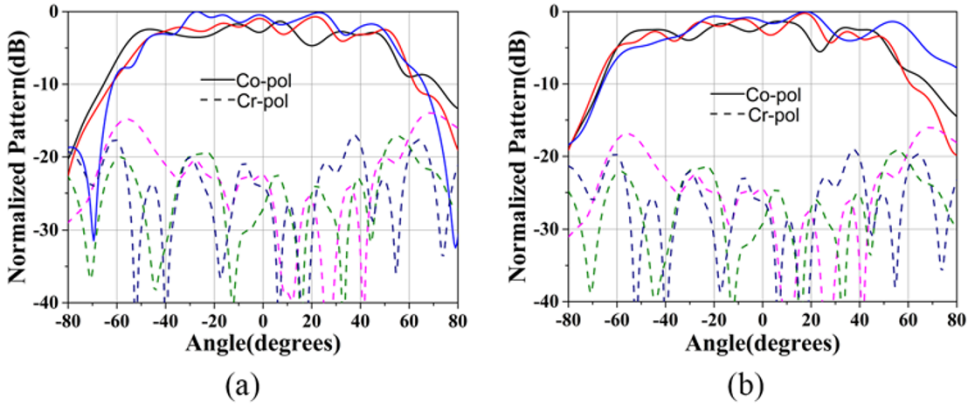


Figure 11. Measured normalized co-polarization and cross-polarization patterns of the element. (a) AZ-plane and (b) EL-plane.

82 (Row 4, Column 14), whose locations are indicated in Fig. 9. As shown in Fig. 10, all measured values remain below 2.6. As expected, the edge elements exhibit higher active VSWR than the center element due to array truncation effects. Furthermore, the active VSWR of the center elements is comparable to the results presented in Fig. 2.

Figure 11 presents the measured normalized co- and cross-polarization patterns of the center element in both the AZ-plane and EL-plane at 32 GHz, 36 GHz, and 40 GHz. The element demonstrates wide beamwidth and low cross-polarization, beneficial for achieving wide-angle scanning with low gain loss.

Figure 12 shows the measured normalized radiation patterns for both H- and V-polarization components. A Taylor amplitude weighting was applied to the array elements via the T/R modules to suppress sidelobes. As a result, the measured sidelobes are significantly lower than the −13.5 dB level of a uniform array, measuring below −23 dB in the AZ-plane and below −18 dB in the EL-plane at broadside.

https://doi.org/10.1017/S1759078726103092 Published online by Cambridge University Press

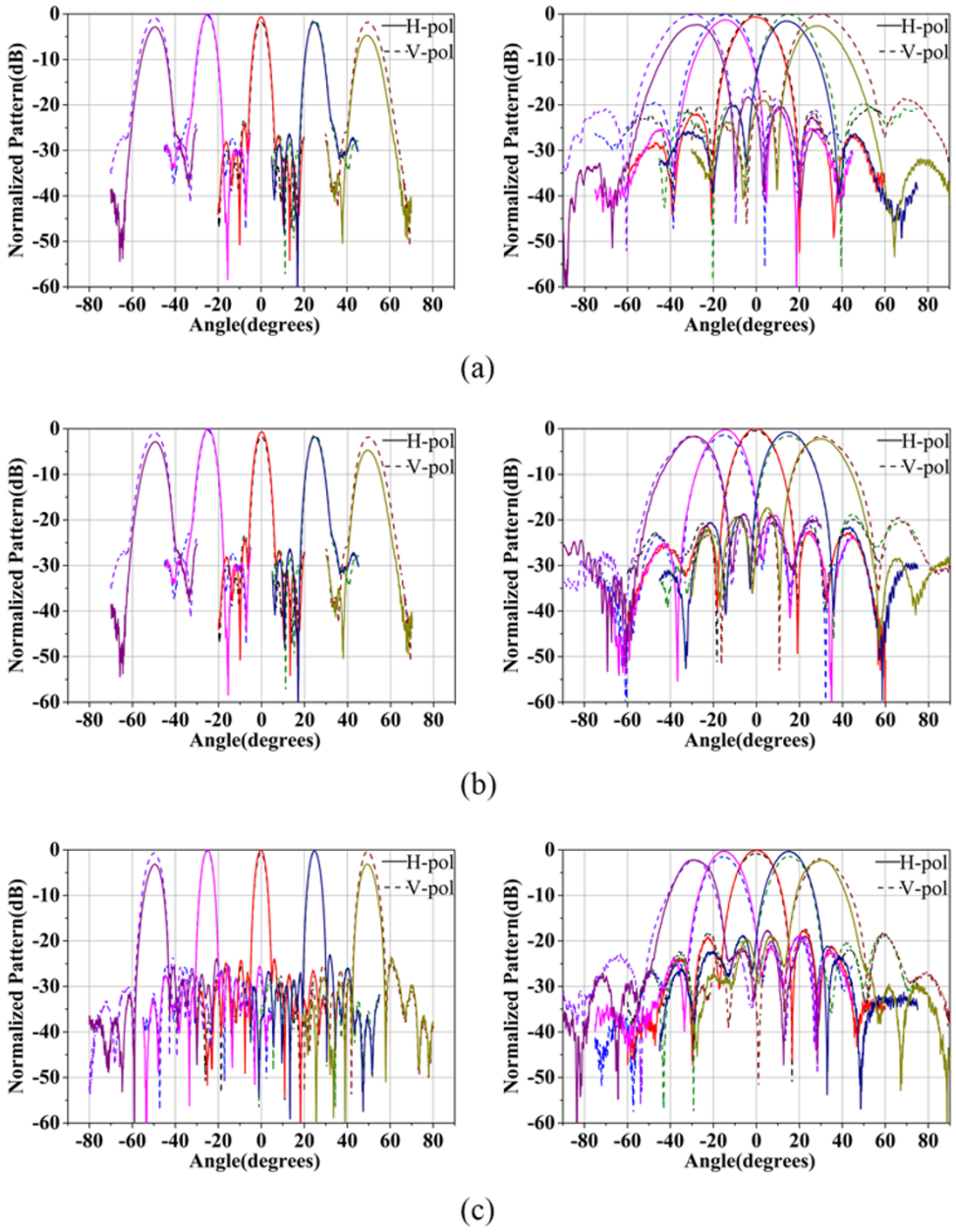


Figure 12. Measured normalized patterns at broadside and scan angles of ±25° and ±50° in the AZ-plane and ±15° and ±30° in the EL-plane. (a) 32 GHz in AZ-plane (left) and EL-plane (right), (b) 36 GHz in AZ-plane (left) and EL-plane (right), and (c) 40 GHz in AZ-plane (left) and EL-plane (right).

For broadside radiation, the H- and V-pol patterns are nearly identical across the band, in good agreement with simulation. The measured amplitude difference between the two components over the scanning range remains within 2.9 dB. Although the simulated amplitude difference is slightly lower than this measured value, the discrepancy is typical and attributable to the finite phase (5.625°) and amplitude (0.5 dB) quantization steps of the practical T/R modules. Overall, the results confirm the array's desirable 45° slant polarization performance.

Figure 13 presents a comparison of the simulated and measured array gain. The measured values are consistently lower, with a maximum observed discrepancy of 1.1 dB. This deviation is attributed primarily to dielectric and conductor losses, as well as to amplitude and phase variations across the array elements.

The measured scanning gain loss for the 28 × 6 array is presented in Table 2. The results indicate a maximum loss of 3 dB across the operating band.

Table 3 compares the performance of the proposed array with prior slant-polarized designs. References [18, 19], and this work employ a polarizer to achieve 45° slant polarization, whereas References [8, 9], and [11] utilize arrays of slant-polarized radiating elements. Although adding a polarizer increases structural complexity and profile height, it enables the array to maintain high polarization purity – specifically, a low amplitude difference between H- and V-pol components – over a wide scan range. Among polarizer-based designs, Reference [18] offers wide bandwidth but is limited to 1D scanning with high scan loss; Reference [19] achieves good polarization purity but over a very

https://doi.org/10.1017/S1759078726103092 Published online by Cambridge University Press

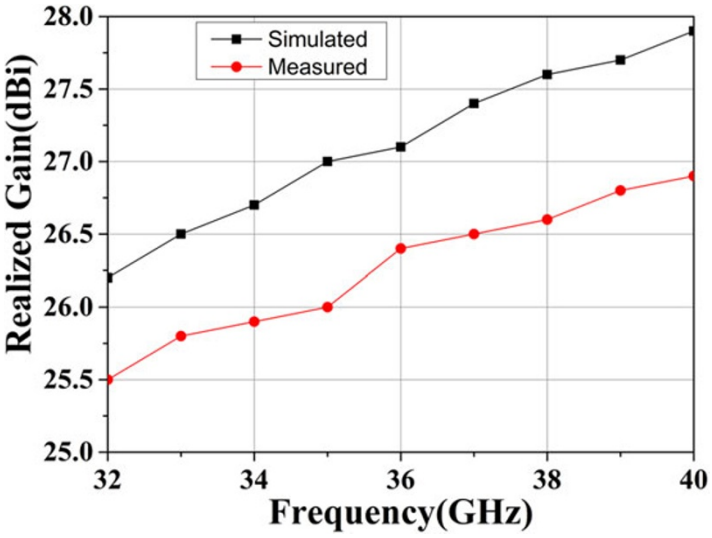


Figure 13. Measured and simulated array gain.

Table 2. Measured gain loss vs. scan angle (dB)

Scan plane		AZ-plane		EL-plane	
Scan angle (degree)		+50	−50	+30	−30
Freq. (GHz)	32	2.1	2.5	0.8	0.6
	36	2.9	3	0.7	0.8
	40	1.8	2.1	0.6	0.5

Table 3. Comparison between reported and proposed slant-polarized antenna arrays

Ref.	Freq. (GHz)	Antenna type	No. of elements	Approach to realizing slant polarization	Gain (dBi)	Scanning range in two dimensions	Gain loss	Max. |H-pol-V-pol|
[8]	26.5–29.5	Gap waveguide	16 × 16	Slant-polarized element	≥27.5	±60° (AZ) ± 10° (EL)	N.A.	N.A.
[9]	0.85–2.25	Wide-slot antenna	1 × 4	Slant-polarized element	≥11.4	N.A.	N.A.	N.A.
[11]	26–30	Patch	8 × 8	Slant-polarized element	N.A.	±55° (AZ) ± 55° (EL)	5.5 dB (AZ) 7.8 dB (EL)	N.A.
[18]	6–18	Double-ridged horn	1 × 16	Three-layer polarizer	≥14.5	±45° (AZ)	4.5 dB (AZ)	N.A.
[19]	6.5–7.5	Patch	1 × 8	Five-layer polarizer	≥14.5	N.A.	N.A.	1.77 dB (at broadside)
This work	32–40	Metal Vivaldi	28 × 6	Two-layer polarizer	≥25.5	±50° (AZ) ± 30° (EL)	3.0 dB (AZ) 0.8 dB (EL)	2.9 dB (±50°, AZ) 2.5 dB (±30°, EL)

narrow bandwidth and without scan analysis. Among designs using slant-polarized elements, Reference [11] attains a relatively wider scan range but suffers from high scan loss and narrow bandwidth, while Reference [8] is outperformed by the proposed design in both bandwidth and elevation-plane scan range, and Reference [9], while offering wider bandwidth, provides no beam scanning analysis. Notably, to the authors' knowledge, no similar polarizer-integrated 2D millimeter-wave phased array has been reported for practical engineering applications. The proposed array demonstrates well-balanced performance in gain, scan loss, and slant polarization purity.

Conclusion

Based on specific practical requirements, this paper presents a Ka-band 2D phased array antenna with 45° slant polarization. The array is modularly constructed from 28 six-element linear sub-arrays. To the best of our knowledge, a polarizer-integrated 2D phased array for practical engineering applications in this band has not been previously reported. The proposed design achieves an active VSWR below 2.6 across the 32–40 GHz band and demonstrates excellent scanning performance of ±50° in azimuth and ±30° in elevation. It maintains a gain over 25.5 dBi with a scan loss

https://doi.org/10.1017/S1759078726103092 Published online by Cambridge University Press

below 3 dB. Moreover, it exhibits remarkable polarization characteristics, with the amplitude difference between H-pol and V-pol components remaining within 2.9 dB throughout the scanning range.

Competing interests. The authors report no conflict of interest.

References

1. **Lindmark B and Nilsson M** (2001) On the available diversity gain from different dual-polarized antennas. *IEEE Journal on Selected Areas in Communications* **19**, 287–294. https://doi.org/10.1109/49.914506.
2. **Wang C, Zhang X and Jin M** (2024) Design of a broadband slant polarized cavity backed microstrip-fed antennas. In *2024 14th International Symposium on Antennas, Propagation and EM Theory (ISAPE)*. Hefei, China: IEEE, pp. 1–4. https://doi.org/10.1109/ISAPE62431.2024.10840407.
3. **Yang Y, Feng Y, Zhang L-K, Xing Z and Li J** (2024) Design of a dual-polarized wide-angle scanning planar phased array antenna. *IEEE Antennas and Wireless Propagation Letters* **23**, 4074–4078. https://doi.org/10.1109/LAWP.2024.3428515.
4. **Jiang K, Zhang W and Zhang Z** (2025) A slant-polarized ultra-wideband all-mental antenna array for wide-angle scanning. In *International Conference on Microwave and Millimeter Wave Technology (ICMMT)*. Xi'an, China: IEEE, pp. 1–3. https://doi.org/10.1109/ICMMT65948.2025.11187739.
5. **Masoumi R, Kazemi R and Fathy AE** (2025) Design and implementation of a slant polarized wideband Vivaldi antenna array feed for monopulse radar reflectors. In *2025 IEEE Radio and Wireless Symposium (RWS)*. San Juan, PR, USA: IEEE, pp. 33–36. https://doi.org/10.1109/RWS62086.2025.10904835.
6. **Chang L, Cao B, Chen L and Zhang J** (2021) Design of a 45° slant-polarized tightly coupled dipole array. In *International Conference on Microwave and Millimeter Wave Technology (ICMMT)*. Nanjing, China: IEEE, pp. 1–3. https://doi.org/10.1109/ICMMT52847.2021.9618343.
7. **Li Z, Li X and Wan C** (2020) Design of a Ka-band slant polarized circular waveguide phased array antenna. In *2020 9th Asia-Pacific Conference on Antennas and Propagation (APCAP)*. Xiamen, China: IEEE, pp. 1–2. https://doi.org/10.1109/APCAP50217.2020.9246144.
8. **Bagheri A, Karlsson H, Bencivenni C, Gustafsson M, Emanuelsson T, Hasselblad M and Alayón Glazunov A** (2023) A 16 × 16 45° slant-polarized gapwaveguide phased array with 65-dBm EIRP at 28 GHz. *IEEE Transactions on Antennas and Propagation* **71**, 1319–1329. https://doi.org/10.1109/TAP.2022.3227718.
9. **Keshavarz R, Winson D, Lipman J, Abolhasan M and Shariati N.** (2023) Slant-polarized MIMO antenna set for vehicular communication. In *2023 17th European Conference on Antennas and Propagation (EuCAP)*. Florence, Italy: IEEE, pp. 1–5. https://doi.org/10.23919/EuCAP57121.2023.10133527.
10. **Lim TH, Park S, Lee CS, Park J and Choo H** (2021) A broadband dual-slant polarized metal Vivaldi antenna for a high-power jammer. In *International Symposium on Antennas and Propagation (ISAP)*. Osaka, Japan: IEEE, pp. 485–486. https://doi.org/10.23919/ISAP47053.2021.9391471.
11. **Chieh J-CS, Yeo E, Kerber M, Olsen R, Merulla E and Sharma S** (2019) A 28 GHz dual slant polarized phased array using silicon beamforming chipsets. In *2019 IEEE International Symposium on Phased*. Waltham, MA, USA: Array System & Technology (PAST). https://doi.org/10.1109/PAST43306.2019.9020837.
12. **Komandla MV, Mishra G and Sharma SK** (2017) Investigations on dual slant polarized cavity-backed massive MIMO antenna panel with beamforming. *IEEE Transactions on Antennas and Propagation* **65**, 6794–6799. https://doi.org/10.1109/TAP.2017.2748239.
13. **Tanha MA, Khalily M and Xiao P** (2019) Slant polarised crossed bow-tie antenna array with reduced number of phase shifters and an embedded feed network. In *IEEE-APS Topical Conference on Antennas and Propagation in Wireless Communications (APWC)*. Granada, Spain: IEEE, pp. 229–231. https://doi.org/10.1109/APWC.2019.8870496.
14. **Kindt RW and Binder BT** (2021) Dual-polarized Vivaldi array on a triangular lattice. *IEEE Transactions on Antennas and Propagation* **69**, 2083–2091. https://doi.org/10.1109/TAP.2020.3037691.
15. **Quan X, Li R, Fan Y and Anagnostou DE** (2014) Analysis and design of a 45° slant-polarized omnidirectional antenna. *IEEE Transactions on Antennas and Propagation* **62**, 86–93. https://doi.org/10.1109/TAP.2013.2288367.
16. **Pan YM, Zheng SY and Hu BJ** (2014) Singly-fed wideband 45° slant-polarized omnidirectional antennas. *IEEE Antennas and Wireless Propagation Letters*, **13**, 1445–1448. https://doi.org/10.1109/LAWP.2014.2341240.
17. **Dastranj A and Abbasi-Arand B** (2016) High-performance 45° slant-polarized omnidirectional antenna for 2–66-GHz UWB applications. *IEEE Transactions on Antennas and Propagation* **64**, 815–820. https://doi.org/10.1109/TAP.2015.2509010.
18. **Yang Y, Zhang F, Zhao J and Zhang C** (2021) An ultra-wideband wide-scanning phased array of double-ridged horn elements with slant polarized characteristics. *Microwave and Optical Technology Letters* **63**, 1532–1537. https://doi.org/10.1002/mop.32788.
19. **Surmeli K and Kizilay A** (2019) Design of slant polariser for directional antennas and antenna arrays. *IET Microwaves, Antennas & Propagation* **13**, 1546–1553. https://doi.org/10.1049/iet-map.2018.5466.
20. **Tao J, Li X, Teng F, Dong R, Li X, Zhu S and Li Y** (2025) ±45° dual-slant polarized all-metal Vivaldi array with isosceles triangular lattice. *Electromagnetics* **45**, 1–17. https://doi.org/10.1080/02726343.2025.2566765.
21. **Ma X, Chai S, Xiao K and Ding L** (2018) Design of all-metal Vivaldi phased array antenna. In *IEEE 3rd International Conference on Signal and Image Processing (ICSIP)*. Shenzhen, China: IEEE, pp. 547–551. https://doi.org/10.1109/SIPROCESS.2018.8600487.
22. **Shin J and Schaubert DH** (1999) A parameter study of stripline-fed Vivaldi notch-antenna arrays. *IEEE Transactions on Antennas and Propagation* **47**, 879–886. https://doi.org/10.1109/8.774151.
23. **Marchand N** (1944) Transmission-line conversion transformers. *Electronics* **17**, 142–146.
24. **Kindt RW and Pickles WR** (2010) Ultrawideband all-metal flared-notch array radiator. *IEEE Transactions on Antennas and Propagation* **58**, 3568–3575. https://doi.org/10.1109/TAP.2010.2071360.
25. **Kindt RW and Logan JT** (2018) Benchmarking ultrawideband phased antenna arrays. *IEEE Antennas and Propagation Magazine* **60**, 34–47. https://doi.org/10.1109/MAP.2018.2818464.
26. **Yan J-B, Gogineni S, Camps-Raga B and Brozena J** (2016) A dual-polarized 2–18-GHz Vivaldi array for airborne radar measurements of snow. *IEEE Transactions on Antennas and Propagation* **64**, 781–785. https://doi.org/10.1109/TAP.2015.2506734.
27. **Ma L, Guan L, Li T, Fan Z and Chen R** (2018) Ultra-wideband all-metal Vivaldi phased array antenna with metal baffles. In *International Applied Computational Electromagnetics Society Symposium - China (ACES)*. Beijing, China: IEEE, pp. 1–2. https://doi.org/10.23919/ACESS.2018.8669245.

https://doi.org/10.1017/S1759078726103092 Published online by Cambridge University Press



Ganlin Feng received the M.S. degree in the School of Electronics and Information, Northwestern Polytechnical University in 2019. He is currently working as an antenna designer in the Department of Microwave Engineering at the Xi'an Electronic Engineering Research Institute. His research focuses on array antenna design.



Junfeng Shi is a Professor-level Senior Engineer. He received his M.S. degree from Xi'an Electronic Engineering Research Institute in 2012 and is currently pursuing an Engineering Doctorate degree. He works at Xi'an Electronic Engineering Research Institute, with his research focusing on array antennas and active phased array design.



Yifei Mu received the M.S. degree from the School of Electronics and Information, Northwestern Polytechnical University in 2019. He is currently working in the Department of Microwave Engineering at the Xi'an Electronic Engineering Research Institute. His research focuses on array antenna design.



Huan Yang is a Senior Engineer. He received his M.S. degree from the College of Electronic and Information Engineering, Nanjing University of Aeronautics and Astronautics in 2014. He is currently working in the Department of Microwave Engineering at the Xi'an Electronic Engineering Research Institute. His research focuses on RF antenna design and RF dynamic sensing system design.



Xingfan Wu received his M.S. degree from the School of Mechano-Electronic Engineering, Xidian University in 2020. He is currently working in the Department of Microwave Engineering at the Xi'an Electronic Engineering Research Institute. His research focuses on radar structure design.



Jiawei Xu received the M.S. degree from the School of Electronic Science and Engineering, University of Electronic Science and Technology of China in 2024. He is currently working in the Department of Microwave Engineering at the Xi'an Electronic Engineering Research Institute. His research focuses on wideband and ultra-wideband antenna design.

https://doi.org/10.1017/S1759078726103092 Published online by Cambridge University Press